

Research Article

Open Access



The influence of A/B-sites doping on antiferroelectricity of PZO energy storage films

Dongxu Li¹, Qinghu Guo², Minghe Cao¹, Zhonghua Yao^{1,2}, Hanxing Liu¹, Hua Hao^{1,2}

¹State Key Laboratory of Advanced Technology for Materials Synthesis and Processing, School of Material Science and Engineering, International School of Material Science and Engineering, Wuhan University of Technology, Wuhan 430070, Hubei, China.

²Foshan Xianhu Laboratory of the Advanced Energy Science and Technology Guangdong Laboratory, Xianhu Hydrogen Valley, Foshan 528200, Guangdong, China.

Correspondence to: Prof. Hua Hao, State Key Laboratory of Advanced Technology for Materials Synthesis and Processing, School of Material Science and Engineering, International School of Material Science and Engineering, Wuhan University of Technology, Wuhan 430070, Hubei, China; Foshan Xianhu Laboratory of the Advanced Energy Science and Technology Guangdong Laboratory, Xianhu Hydrogen Valley, Foshan 528200, Guangdong, China. E-mail: haohua@whut.edu.cn

How to cite this article: Li D, Guo Q, Cao M, Yao Z, Liu H, Hao H. The influence of A/B-sites doping on antiferroelectricity of PZO energy storage films. *Microstructures* 2023;3:2023007. <https://dx.doi.org/10.20517/microstructures.2022.27>

Received: 22 Sep 2022 **First Decision:** 2 Nov 2022 **Revised:** 13 Nov 2022 **Accepted:** 7 Dec 2022 **Published:** 10 Jan 2023

Academic Editors: Ruzhong Zuo, Shiqing Deng **Copy Editor:** Fangling Lan **Production Editor:** Fangling Lan

Abstract

Antiferroelectrics are a kind of unique dielectric materials, mainly due to their polarization behavior, and composition-induced antiferroelectricity stability also draws considerable attention. In this work, single orthorhombic phase ($\text{Pb}_{0.95}\text{Bi}_{0.05}\text{ZrO}_3$ (PBZ), $\text{Pb}(\text{Zr}_{0.95}\text{Bi}_{0.05})\text{O}_3$ (PZB), and PbZrO_3 (PZO) films with good density and flatten surface was prepared on Pt/Ti/SiO₂/Si substrate via sol-gel method. Compared with pure PZO films, the PBZ and PZB films possess increased switching electric field difference ΔE due to enhanced forward switching field and the late response of backward switching field. In terms of stabilizing AFE phase, changing the tolerance factor t has the similar effect as Bi-doping the A/B sites in PZO, with the modification of the A-site being more effective than that of the B-site. PBZ films achieve a high recoverable energy density (W_{rec}) of 26.4 J/cm³ with energy efficiency (η) of 56.2% under an electric field of 1278 kV/cm, which exceeds other pure AFE materials. This work provides a fundamental understanding of the crystal structure-related antiferroelectricity of PZO materials and broadens the chemical doping route to enhance the electric properties of AFE materials.

Keywords: Antiferroelectrics, energy storage, PbZrO_3 , thin film, switching field



© The Author(s) 2023. **Open Access** This article is licensed under a Creative Commons Attribution 4.0 International License (<https://creativecommons.org/licenses/by/4.0/>), which permits unrestricted use, sharing, adaptation, distribution and reproduction in any medium or format, for any purpose, even commercially, as long as you give appropriate credit to the original author(s) and the source, provide a link to the Creative Commons license, and indicate if changes were made.



INTRODUCTION

Dielectric materials, an essential part of capacitors, would generate polarization under an electric field, enabling them to be widely used in electrocaloric, actuator, and energy storage devices. According to different polarization behaviors, dielectrics can be divided into linear dielectrics (LDs), ferroelectrics (FEs), and antiferroelectrics (AFEs)^[1-4]. The energy storage performances of dielectric materials could be determined by the polarization-electric field (P - E) curves as follow:

$$W_{\text{rec}} = \int_{P_r}^{P_{\text{max}}} E dP \quad (1)$$

$$\eta = \frac{W_{\text{rec}}}{W_{\text{rec}} + W_{\text{loss}}} \quad (2)$$

where W_{rec} , η , W_{loss} , P_{max} , and P_r are the recoverable energy density, the energy efficiency, the dissipated energy, the maximum polarization, and the remnant polarization under an applied electric field E , respectively. Therefore, FE and AFE materials are suitable for energy storage applications due to a large P_{max} , low P_r , and moderate E . Meanwhile, dielectric films with much larger breakdown strength E_b could attain higher energy density than their bulk counterparts^[3-6].

AFE materials possess a characteristic known as a double hysteresis loop, which corresponds to four current peaks under an applied electric field. The current peaks represent the AFE-to-FE phase transition at forward switching field E_f and FE-to-AFE phase transition at backward switching field E_A , respectively^[7-10]. PbZrO_3 (PZO), as a prototype AFE material, exhibits an apparent double hysteresis loop characteristic, while the antiferroelectricity's origin is still controversial^[11,12]. Hao *et al.* used the tolerance factor (t) to evaluate the antiferroelectricity of PZO films, and later an increasing researches focus on chemical doping to adjust antiferroelectricity of Pb-based and Pb-free AFE materials using t value^[13]. The equation of tolerance factor (t) of perovskite structure can be expressed as follow:

$$t = \frac{r_{A^+} + r_O}{\sqrt{2}(r_B + r_O)} \quad (3)$$

where r_A , r_B and r_O denote the ion radius of A-site, B-site, and oxygen, respectively. It is accepted that the AFE phase is stabilized at $t < 1$, and the FE phase is stabilized at $t > 1$. For example, a reduced t value can be found in La-doped PZO and Ca-doped AgNbO_3 materials corresponding to an enhanced E_f and E_A to stabilize the AFE phase^[14,15]. In 2017, Zhao *et al.* prepared $\text{Ag}(\text{Nb}_{1-x}\text{Ta}_x)\text{O}_3$ ceramics in a similar t value and proposed that enhanced antiferroelectricity should be attributed to reduced polarizability of the B-site^[10]. In addition, (Ca, Zr), (Sr, Zr) and (Ca, Hf) modified NaNbO_3 AFE ceramics both possess a double hysteresis loop by decreasing the value of t while keeping the value of electronegativity fixed^[16-18]. It can be seen that the electric field-induced AFE phase could be affected by a tolerance factor, polarizability, and electronegativity in A/B-sites for Pb-based and Pb-free materials. In the case of only considering the tolerance factor t , whether the role of A/B-sites on influencing antiferroelectricity of PZO films exists difference.

Following the above discussion, we choose Bi^{3+} (~ 1.38 Å for CN = 12 and 1.03 Å for CN = 6) to replace Pb^{2+} (1.49 Å for CN = 12) and Zr^{4+} (0.72 Å for CN = 6) at A/B-sites respectively^[19], compare the difference of A/B-sites on influencing antiferroelectricity of PZO, and hence fabricate $(\text{Pb}_{0.95}\text{Bi}_{0.05})\text{ZrO}_3$ (PBZ), $\text{Pb}(\text{Zr}_{0.95}\text{Bi}_{0.05})\text{O}_3$ (PZB) and pure PbZrO_3 (PZO) films. A schematic representation of the crystal structure of the Bi-doping PZO material can be seen in [Figure 1](#). Based on Equation (3), calculated t values are 0.9639,

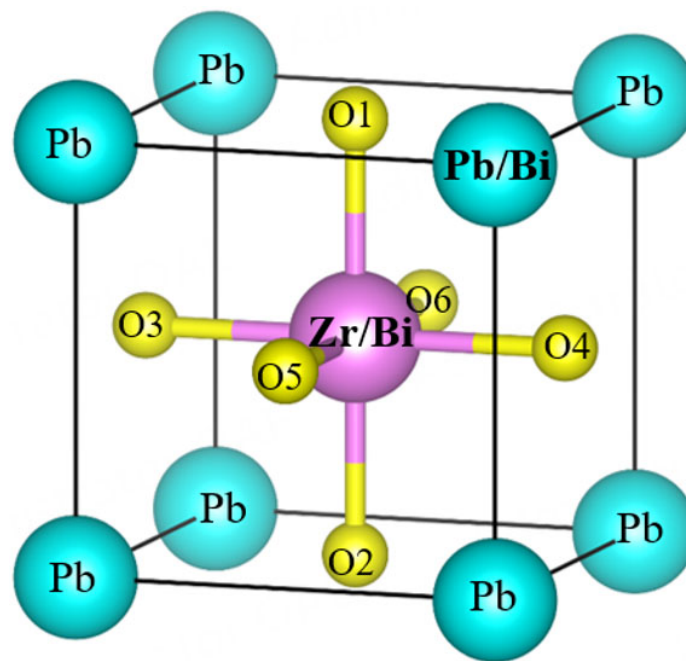


Figure 1. The schematic of 5 mol% Bi^{3+} replaces Pb^{2+} at A-site and Zr^{4+} at the B-site of PZO. PZO: PbZrO_3 .

0.9621, and 0.9569 for PZO, PBZ, and PZB compositions, respectively. Meanwhile, a correlation between the tolerance factor t and the stabilized antiferroelectricity of PZO is discussed. Our work provides a new perspective in improving energy storage properties of AFE materials and prompts the development of AFE materials.

MATERIALS AND METHODS

$(\text{Pb}_{0.95}\text{Bi}_{0.05})\text{ZrO}_3$ (PBZ), $\text{Pb}(\text{Zr}_{0.95}\text{Bi}_{0.05})\text{O}_3$ (PZB), and pure PbZrO_3 (PZO) films were prepared on 150-nm Pt/20-nm Ti/100-nm SiO_2/Si substrate via sol-gel method. $\text{Pb}(\text{CH}_3\text{COO})_2 \cdot 3\text{H}_2\text{O}$ (AR, 99.5%), $\text{Bi}(\text{NO}_3)_3 \cdot 3\text{H}_2\text{O}$ (AR, 99%), and $\text{Zr}(\text{OCH}_2\text{CH}_2\text{CH}_3)_4$ solution (70 wt%) were used as starting raw materials to prepare a stable 0.2 M precursor solution. Simultaneously, 2-methoxyethanol, acetic acid, and acetylacetonone were used as solvents and stabilizers. A 10% excess lead was added to the solvent to compensate for lead loss during the annealing process. The completed sol was spin-coated on the substrate at 4500 rpm for 30 s, pyrolyzed at 450 °C, and annealed at 650 °C to attain the desired thickness. The annealing process was achieved using an RTP-500 furnace in an air atmosphere. Finally, a P_i electrode with a diameter of ~200 μm was deposited through a magnetron sputtering system.

The crystal phase of PZO-based films was examined by grazing incident X-ray diffraction (GIXRD, Empyrean, PANalytical, Netherlands) with $\text{Cu K}\alpha_1$ radiation. The cross-section morphology of the PZO-based thin films was measured using a field emission scanning electron microscope (SEM, Zeiss Ultra Plus, Germany). The surface information of thin films was collected by atomic force microscopy (AFM, Nanoscope IV, Veeco, USA). The thicknesses of PZO-based films are about 180 nm. The dielectric and ferroelectric properties of the PZO-based thin films were measured using an impedance analyzer (Agilent 4294) and a ferroelectric workstation (Precision Premier II, Radiant Technologies Inc., USA).

RESULTS AND DISCUSSION

Figure 2A shows the GIXRD patterns of PZO-based films at $2\theta = 20^\circ\text{-}60^\circ$. In the case of a PZO-based film with good crystallinity, the perovskite crystalline structure is orthorhombic phase, and no secondary phase is detectable in the range of accuracy of GIXRD technology. In order to investigate the effect of Bi doping in PZO, the enlarged patterns of PZO-based films at $2\theta = 30^\circ\text{-}31^\circ$ are shown in Figure 2B. The diffraction peak (122) around 30.5° of PBZ and PZB compared to pure PZO has a slight shift towards the low angle and high angle, respectively, which demonstrates Bi successfully replaces Pb and Zr at A/B-sites. In terms of the change in diffraction peak, similar phenomena have been observed in La-doped PZO films at low content^[15].

Figure 3A shows the SEM images of PZO-based films. It can be seen that all films possess good density and no pores and crack in the surface morphology. The grain size of PZB films exceeds PBZ and pure PZO films, which should be related to a reduced Pb/Zr ratio compared to PZO and PBZ. Figure 3B displays the AFM images of PZO-based films. The surface roughness R_q is 2.91 nm, 3.32 nm, and 4.04 nm for pure PZO, PBZ, and PZB films. PZO-based thin films are characterized by a smooth and flattened surface, indicating high-quality materials.

Due to the valence difference of Bi^{3+} , Pb^{2+} and Zr^{4+} , the chemical defect would be generated. The defect equation of Bi replaces Pb and Zr is given as follows:



It can be seen that the point defect of $V_{\text{pb}}^{\cdot\cdot}$ and $V_{\text{O}}^{\cdot\cdot}$ could be generated when Bi acts as a donor and acceptor dopant, respectively. Figure 4 shows the room temperature frequency dependency of dielectric properties for PZO-based films. As frequency increases, the dielectric properties of PZO-based films maintain stability over the frequency range of 1 kHz-1 MHz. Figure 4A shows that the dielectric constant enhances from ~ 250 for PZO films to ~ 325 for PBZ and PZB films, which may be related to an increased point defect contribution. In addition, Figure 4B illustrates that the dielectric losses of PZO-based films are around 0.1.

Figure 5A shows the room temperature P - E loops of PZO-based films at an applied electric field of 800 kV/cm. PZO films exhibit an apparent double hysteresis loop. Bi-doped PZO films at A/B sites still show double hysteresis loops, but the polarization and switching fields have been changed. The polarization differences ΔP between P_{max} and P_r of PZO-based films are exhibited in Figure 5C. The P_r of all PZO-based films is unchanged, but the P_{max} of Bi-doped PZO films is lower than that of pure PZO films. Therefore, ΔP of Bi-doped PZO films cannot be enhanced effectively at the same electric field. Figure 5B shows the I - E loops of PZO-based films at an applied electric field of 800 kV/cm. Four current peaks correspond to the AFE-to-FE and FE-to-AFE phase transition, respectively^[8,10]. Compared to pure PZO films, PBZ and PZB films both possess a lower current density and higher forward switching field E_r of 562.2 kV/cm for PBZ and 537.3 kV/cm for PZB than 413.5 kV/cm for PZO films, which illustrates Bi-doping enhances antiferroelectricity of PZO materials in some degree. As discussed above, this result may be related to a reduction in t value to stabilize the AFE phase. Unfortunately, the increased ΔE value sacrifices the E_r of PBZ and PZB, as shown in Figure 5D. It can be attributed to an enlarged grain size [Figure 3], which differs from the previous results. As grain size decreases, hysteresis loss in relaxor ferroelectric materials and antiferroelectric materials is reduced due to increased dipole mobility, and therefore PBZ and PZB with large grain sizes would possess a high ΔE . It can be seen that the antiferroelectricity of PZO is no positive

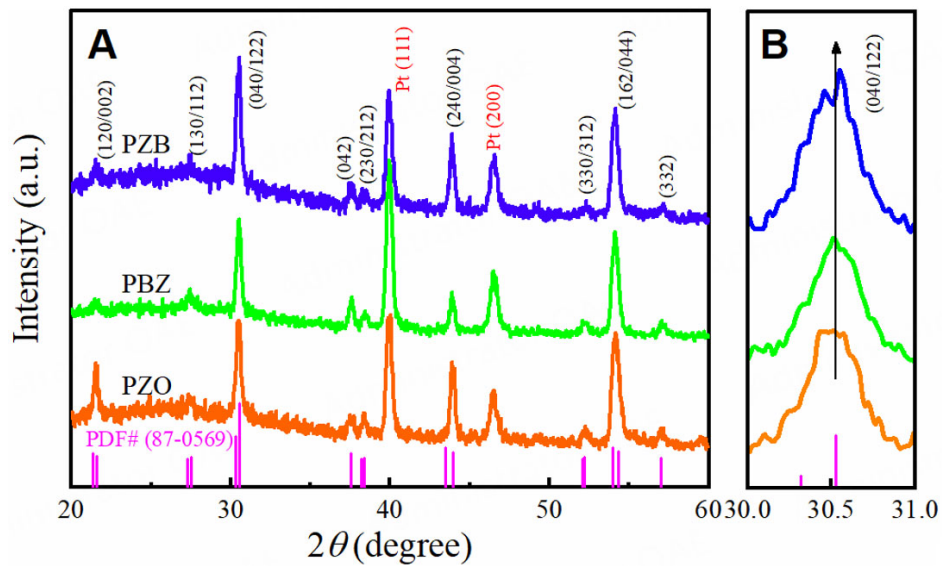


Figure 2. (A) The GIXRD patterns of PZO-based films at 2θ range from 20° to 60° . (B) The enlarged patterns at $2\theta = 30^\circ$ – 31° . GIXRD: Grazing incident X-ray diffraction; PZO: PbZrO_3 .

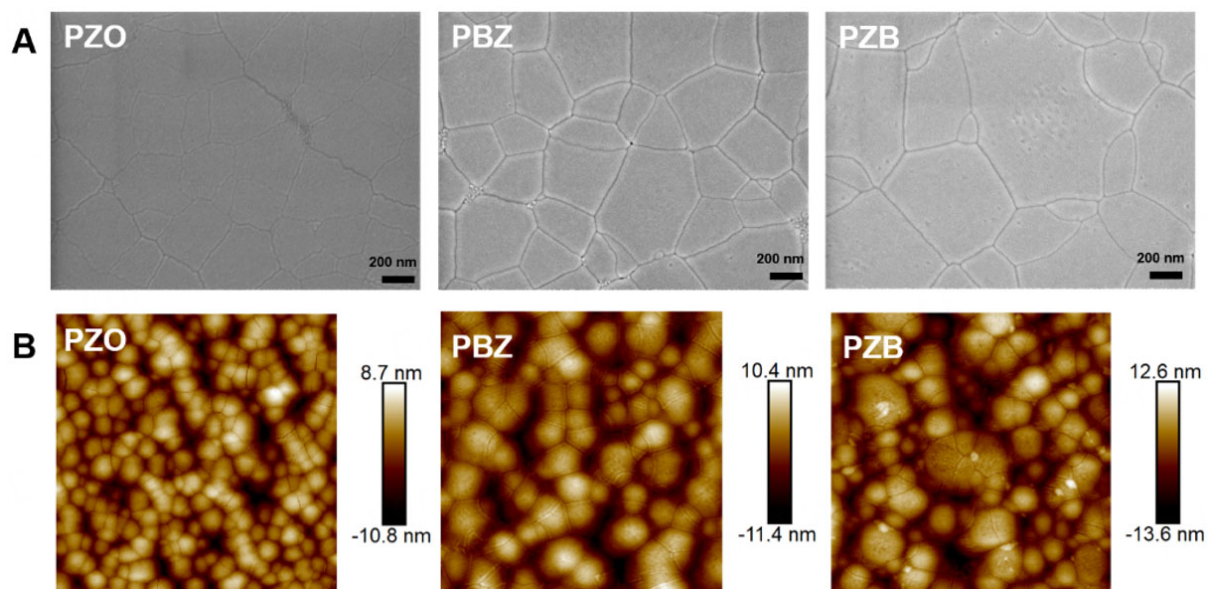


Figure 3. The (A) SEM images and corresponding (B) AFM images ($5 \times 5 \mu\text{m}$) for PZO, PBZ, and PZB films. SEM: Scanning electron microscope; AFM: atomic force microscopy; PZO: PbZrO_3 ; PBZ: $(\text{Pb}_{0.95}\text{Bi}_{0.05})\text{ZrO}_3$; PZB: $\text{Pb}(\text{Zr}_{0.95}\text{Bi}_{0.05})\text{O}_3$.

correlation with the tolerance factor in t in A/B-sites doping. In addition, grain size should be taken into account when enhancing antiferroelectricity.

Figure 6A shows the P - E loops of pure PZO films at different electric fields. As the electric field enhances, linear hysteresis loops gradually transform into double hysteresis loops causing P_{max} to increase dramatically. With further improving the electric field, the P - E loops are unchanged and stay in a polarization saturation state. A detailed description of the division of regions into different states can be found in the following content. For PBZ and PZB films, the polarization saturation has a slight delay. Meanwhile, breakdown

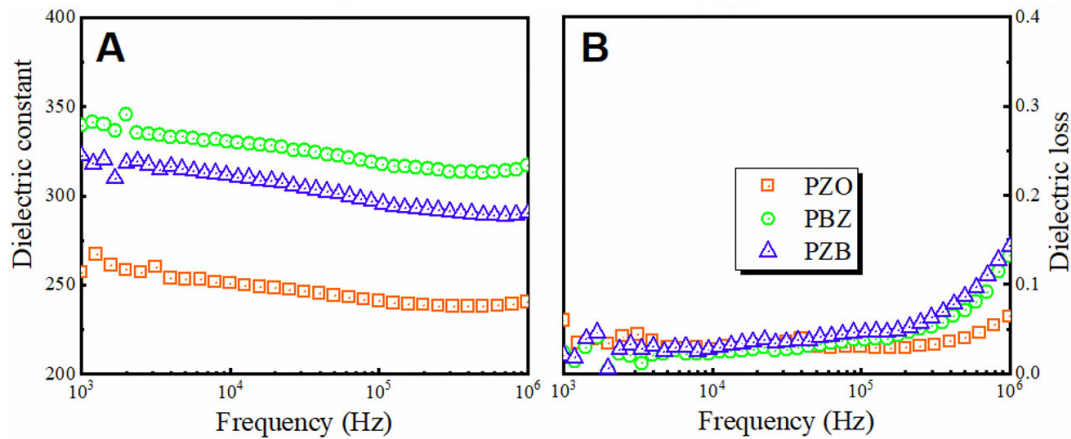


Figure 4. Frequency-dependent (A) dielectric constant and (B) dielectric loss for PZO-based films at room temperature. PZO: PbZrO_3 .

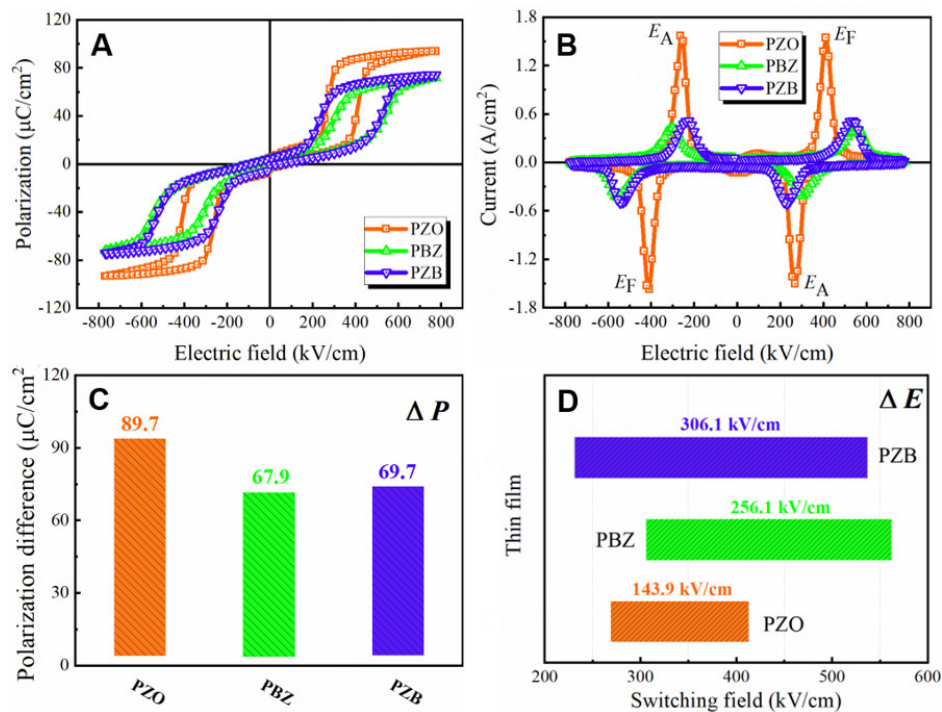


Figure 5. (A) The P - E loops of PZO-based films at 800 kV/cm, and corresponding (C) the polarization difference value of ΔP ($P_{\text{max}} - P_r$). (B) The I - E loops of PZO-based films at 800 kV/cm, and corresponding (D) the switching field value of ΔE ($E_F - E_A$). PZO: PbZrO_3 .

strength enhances compared to pure PZO films, as exhibited in Figure 6B and C. The leakage current is a crucial parameter for evaluating dielectric film's electric properties and conduction mechanisms^[20-23]. Figure 6D illustrates the leakage current for PZO-based films as a function of the electric field. It can be seen that the curve of leakage current of pure PZO films can be divided into two parts: For low electric field, the leakage conductivity belongs to the bulk-limited Ohmic mechanism. The Fowler-Nordheim tunneling (FN) mechanism dominates at high electric field. A similar phenomenon also exists in PBZ and PZB films. Note that the transition field from bulk-limited to FN mechanism gradually reduces for pure PZO, PBZ, and PZB films, which may be related to different defect types in aliovalent doping PZO at A/B sites. Compared to the lead vacancy, the oxygen vacancy may easily contribute more leakage carrier; hence, the transformation field of PZB from Ohmic into FN mechanism reduces compared to PBZ.

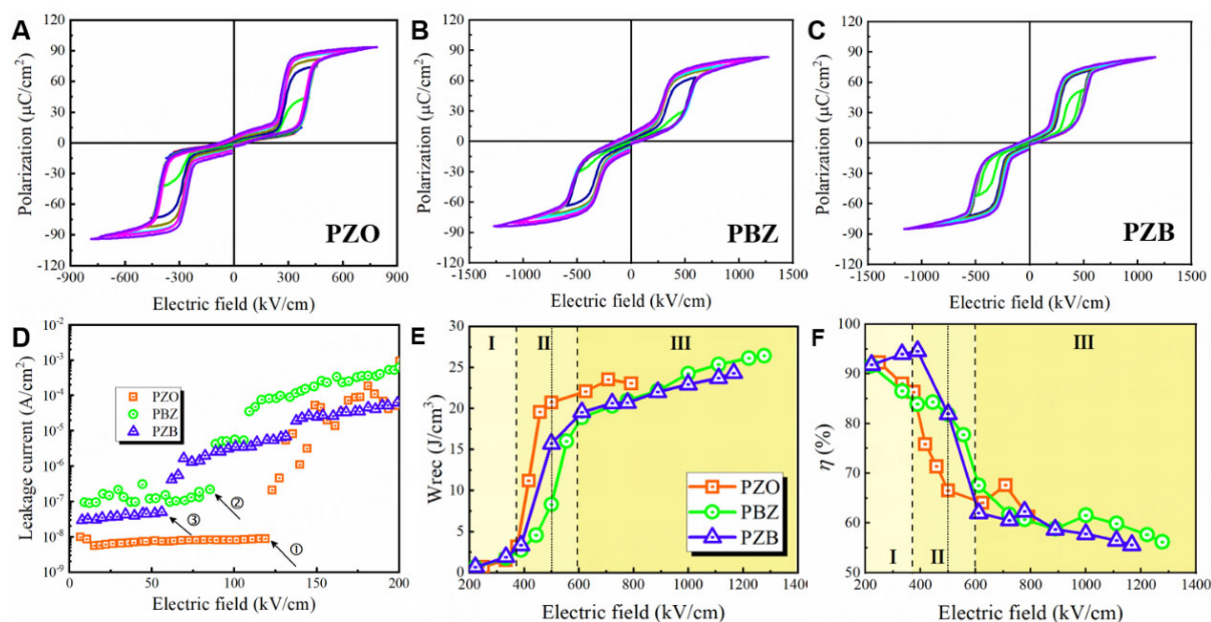


Figure 6. (A-C) The P - E loops of PBZ, PZB, and pure PZO films at different electric fields, respectively. (D) The leakage current functions of electric field for PZO-based films. (E) The recoverable energy density W_{rec} and (F) the energy efficiency η of PZO-based films at an applied electric field. PBZ: $(\text{Pb}_{0.95}\text{Bi}_{0.05})\text{ZrO}_3$; PZB: $\text{Pb}(\text{Zr}_{0.95}\text{Bi}_{0.05})\text{O}_3$; PZO: PbZrO_3 .

Figure 6E shows the recoverable energy density W_{rec} as a function of the electric field for PZO-based films. Similar to other literature^[24], a corresponding curve can be divided into three regions as the electric field increases. For region I, PZO-based films possess a low W_{rec} value, which should belong to the AFE phase stage with a linear polarization curve. For region II, W_{rec} of PZO-based films both sharply enhance, which should correspond to AFE-FE co-existed phase stage. Note that the dashed and dot lines represent different terminal transition fields into region III, which means Bi dope PZO would delay the polarization enhancement. The W_{rec} only slightly enhances into region III, which should be attributed to the polarization saturation phenomenon at the high electric field^[25,26]. The energy efficiency η as functions of electric field for PZO-based films is displayed in Figure 6F. Similarly, the curves of η also could be divided into three regions. As the electric field enhances, the η value gradually decreases and attains a relatively 50%-60% range. PBZ films achieve a maximum W_{rec} of 26.4 J/cm³ with a η of 56.2 %, which exceeds other reported pure AFE materials^[27-29].

It is known that energy storage stability, including temperature and frequency^[5,14,30], is an important parameter for evaluating the material applications, as shown in Figure 7. As temperature enhances, double hysteresis loop characteristics of PBZ films gradually transform into relaxor AFE, as shown in Figure 7A. Meanwhile, the W_{rec} gradually decreases and η value remains essentially unchanged (see Figure 7C), which should be related to the Curie temperature of PZO at about 230 °C, corresponding to the AFE-to-PE phase transition^[8,31]. Figure 7B displayed frequency-dependent P - E loops of PBZ films at room temperature. As frequency enhances, polarization decreases and hysteresis loss also reduces. Therefore, the W_{rec} and η of PBZ films display good frequency stability, as shown in Figure 7D.

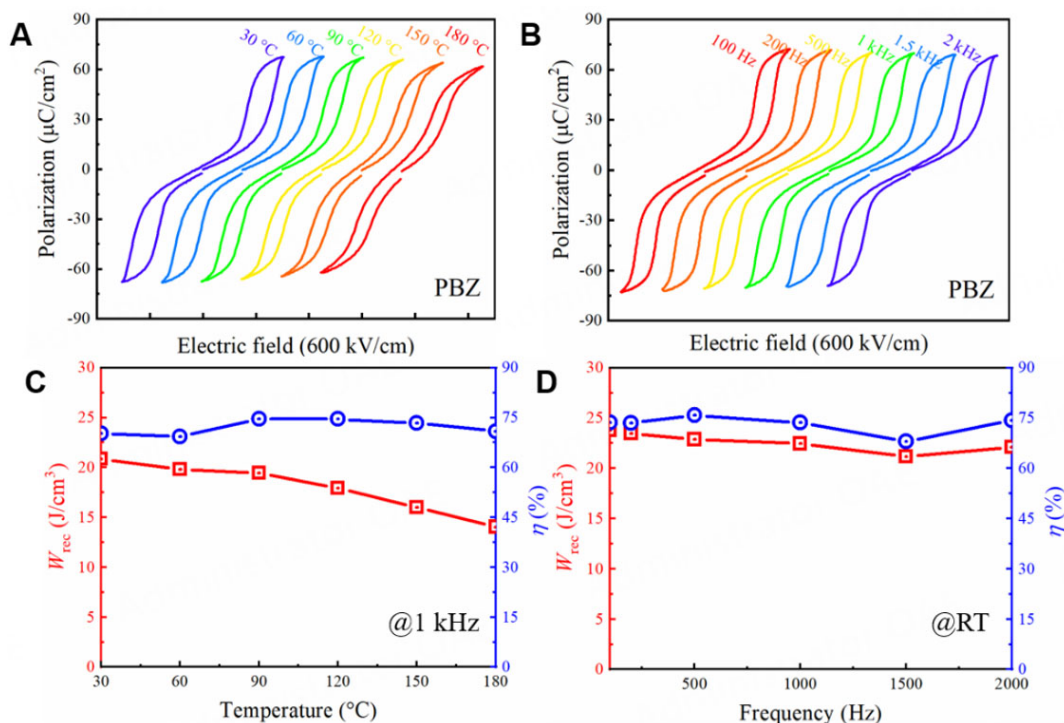


Figure 7. (A) Temperature-dependent P - E loops and corresponding (C) W_{rec} , η of PBZ films at 1 kHz. (B) Frequency-dependent P - E loops and corresponding (D) W_{rec} , η of PBZ films at room temperature. PBZ: $(\text{Pb}_{0.95}\text{Bi}_{0.05})\text{ZrO}_3$.

CONCLUSIONS

PZO, PBZ, and PZB films are prepared on Pt/Ti/SiO₂/Si substrate via the sol-gel method. Crystallized PZO-based films with orthorhombic perovskite phases exhibit low roughness and good density. The dielectric constants of the Bi-doped PZO and pure PZO films are approximately 300, and these films possess good frequency stability at room temperature. Compared to pure PZO films, ΔE value increases and ΔP decrease for PBZ and PZB films hindering the effective energy storage. A/B-site doping in influencing the antiferroelectricity of PZO has a similar effect in only considering t value, and A-site doping would be better than B-site one in energy storage properties. PBZ films achieve a high W_{rec} of 26.4 J/cm³ with a η of 56.2 % under an applied electric field of 1278 kV/cm, accompanying a suitable temperature and frequency energy storage stabilities.

DECLARATIONS

Authors' contributions

Conceived the idea: Li D

Performed the experiments and data analysis: Li D, Guo Q, Cao M, Yao Z, Liu H, Hao H

Provided the technical support: Cao M, Yao Z, Liu H, Hao H

Wrote and reviewed the manuscript: Li D, Hao H

Availability of data and materials

Not applicable.

Financial support and sponsorship

This work was supported by Major Program of the Natural Science Foundation of China (Grant No. 51790490), Foshan Xianhu Laboratory of the Advanced Energy Science and Technology Guangdong

Laboratory (Grant No. XHT2020-011), Sanya Science and Education Innovation Park of Wuhan University of Technology (2020KF0017) and Guangdong Basic and Applied Basic Research Foundation (2022A1515010073).

Conflicts of interest

All authors declared that there are no conflicts of interest.

Ethical approval and consent to participate

Not applicable.

Consent for publication

Not applicable.

Copyright

© The Author(s) 2023.

REFERENCES

1. Yao Z, Song Z, Hao H, et al. Homogeneous/inhomogeneous-structured dielectrics and their energy-storage performances. *Adv Mater* 2017;29:1601727. DOI PubMed
2. Yang L, Kong X, Li F, et al. Perovskite lead-free dielectrics for energy storage applications. *Prog Mater Sci* 2019;102:72-108. DOI
3. Palneedi H, Peddigari M, Hwang G, Jeong D, Ryu J. High-performance dielectric ceramic films for energy storage capacitors: progress and outlook. *Adv Funct Mater* 2018;28:1803665. DOI
4. Li D, Zeng X, Li Z, et al. Progress and perspectives in dielectric energy storage ceramics. *J Adv Ceram* 2021;10:675-703. DOI
5. Pan H, Li F, Liu Y, et al. Ultrahigh-energy density lead-free dielectric films via polymorphic nanodomain design. *Science* 2019;365:578-82. DOI PubMed
6. Qi H, Xie A, Tian A, Zuo R. Superior energy-storage capacitors with simultaneously giant energy density and efficiency using nanodomain engineered BiFeO₃-BaTiO₃-NaNbO₃ lead-free bulk ferroelectrics. *Adv Energy Mater* 2020;10:1903338. DOI
7. Kittel C. Theory of antiferroelectric crystals. *Phys Rev* 1951;82:729-32. DOI
8. Hao X, Zhai J, Kong LB, Xu Z. A comprehensive review on the progress of lead zirconate-based antiferroelectric materials. *Prog Mater Sci* 2014;63:1-57. DOI
9. Randall CA, Fan Z, Reaney I, Chen L, Trolier-mckinstry S. Antiferroelectrics: history, fundamentals, crystal chemistry, crystal structures, size effects, and applications. *J Am Ceram Soc* 2021;104:3775-810. DOI
10. Zhao L, Liu Q, Gao J, Zhang S, Li JF. Lead-free antiferroelectric silver niobate tantalate with high energy storage performance. *Adv Mater* 2017;29:1701824. DOI PubMed
11. Tagantsev AK, Vaideeswaran K, Vakhrushev SB, et al. The origin of antiferroelectricity in PbZrO₃. *Nat Commun* 2013;4:2229. DOI PubMed
12. Aramberri H, Cazorla C, Stengel M, Íñiguez J. On the possibility that PbZrO₃ not be antiferroelectric. *NPJ Comput Mater* 2021;7:196. DOI
13. Hao X, Zhai J, Yao X. Improved energy storage performance and fatigue endurance of Sr-doped PbZrO₃ antiferroelectric thin films. *J Am Ceram Soc* 2009;92:1133-5. DOI
14. Luo N, Han K, Zhuo F, et al. Design for high energy storage density and temperature-insensitive lead-free antiferroelectric ceramics. *J Mater Chem C* 2019;7:4999-5008. DOI
15. Cai H, Yan S, Zhou M, et al. Significantly improved energy storage properties and cycling stability in La-doped PbZrO₃ antiferroelectric thin films by chemical pressure tailoring. *J Eur Ceram Soc* 2019;39:4761-9. DOI
16. Shimizu H, Guo H, Reyes-Lillo SE, Mizuno Y, Rabe KM, Randall CA. Lead-free antiferroelectric: xCaZrO₃-(1-x)NaNbO₃ system (0<x<0.10). *Dalton Trans* 2015;44:10763-72. DOI PubMed
17. Guo H, Shimizu H, Mizuno Y, Randall CA. Strategy for stabilization of the antiferroelectric phase (Pbma) over the metastable ferroelectric phase (P21ma) to establish double loop hysteresis in lead-free (1-x)NaNbO₃-xSrZrO₃ solid solution. *J Appl Phys* 2015;117:214103. DOI
18. Gao L, Guo H, Zhang S, Randall CA. A perovskite lead-free antiferroelectric xCaHfO₃-(1-x)NaNbO₃ with induced double hysteresis loops at room temperature. *J Appl Phys* 2016;120:204102. DOI
19. Shannon RD. Revised effective ionic radii and systematic studies of interatomic distances in halides and chalcogenides. *Acta Cryst A* 1976;32:751-67. DOI
20. Chiu F. A review on conduction mechanisms in dielectric films. *Adv Mater Sci Eng* 2014;2014:1-18. DOI
21. Huang Y, Shu L, Zhang S, et al. Simultaneously achieved high-energy storage density and efficiency in (K,Na)NbO₃-based lead-free

- ferroelectric films. *J Am Ceram Soc* 2021;104:4119-30. DOI
22. Fan Q, Ma C, Ma C, Lu R, Cheng S, Liu M. Manipulating leakage behavior via thickness in epitaxial $\text{BaZr}_{0.35}\text{Ti}_{0.65}\text{O}_3$ thin film capacitors. *Appl Phys Lett* 2020;116:192902. DOI
 23. Jiang X, Lv J, Chen Z, et al. Superior energy storage BaTiO_3 -based amorphous dielectric film with polymorphic hexagonal and cubic nanostructures. *Chem Eng J* 2022;431:133447. DOI
 24. Chen X, Cao F, Zhang H, et al. Dynamic hysteresis and scaling behavior of energy density in $\text{Pb}_{0.99}\text{Nb}_{0.02}[(\text{Zr}_{0.60}\text{Sn}_{0.40})_{0.95}\text{Ti}_{0.05}]\text{O}_3$ antiferroelectric bulk ceramics. *J Am Ceram Soc* 2012;95:1163-6. DOI
 25. Li D, Shen Z, Li Z, et al. Optimization of polarization behavior in (1-x)BSBNT-xNN ceramics for pulsed power capacitors. *J Mater Chem C* 2020;8:7650-7. DOI
 26. Ren Y, Cheng H, Ouyang J, et al. Bimodal polymorphic nanodomains in ferroelectric films for giant energy storage. *Energy Storage Mater* 2022;48:306-13. DOI
 27. Chen MJ, Ning XK, Wang SF, Fu GS. Significant enhancement of energy storage density and polarization in self-assembled PbZrO_3 :NiO nano-columnar composite films. *Nanoscale* 2019;11:1914-20. DOI PubMed
 28. Xu R, Wang M, Zhu Q, Xu Z, Feng Y, Wei X. Investigation on antiferroelectricity of $\text{Pb}_{0.97}\text{La}_{0.02}(\text{Hf}_{1-x}\text{Ti}_x)\text{O}_3$ ceramics with low Ti content ($0 \leq x \leq 0.1$). *J Am Ceram Soc* 2022;105:7438-45. DOI
 29. Huang X, Zhang T, Wang W, Ge P, Tang X. Tailoring energy-storage performance in antiferroelectric PbHfO_3 thin films. *Mater Design* 2021;204:109666. DOI
 30. Jiang X, Hao H, Zhang S, et al. Enhanced energy storage and fast discharge properties of BaTiO_3 based ceramics modified by $\text{Bi}(\text{Mg}_{1/2}\text{Zr}_{1/2})\text{O}_3$. *J Eur Ceram Soc* 2019;39:1103-9. DOI
 31. Li YZ, Wang ZJ, Bai Y, Zhang ZD. High energy storage performance in Ca-doped PbZrO_3 antiferroelectric films. *J Eur Ceram Soc* 2020;40:1285-92. DOI